ADVANCED THERAPEUTICS
www.advtherap.com

A Manganese Phosphate Nanocluster Activates the cGAS-STING Pathway for Enhanced Cancer Immunotherapy

*Min Gao, Yu-Qing Xie, Kewen Lei, Yu Zhao, Armand Kurum, Simon Van Herck, Yugang Guo, Xiaomeng Hu, and Li Tang**

Targeting the stimulator of interferon genes (STING) pathway with cyclic dinucleotides (CDNs), the natural STING agonists, is a promising immunotherapeutic strategy for cancer. However, the clinical application of natural CDNs as therapeutics is greatly hindered by their intrinsic properties including negative charges, small molecular weight, and high susceptibility to enzymatic degradation. Mn^{2+} ions have been recently discovered to directly activate the cyclic GMP-AMP (cGAMP) synthase (cGAS) and augment cGAMP-STING binding affinity. Here, a PEGylated manganese(II) phosphate (MnP-PEG) nanocluster is developed with high biocompatibility and potent capacity to stimulate the cGAS-STING pathway. MnP-PEG nanoclusters activate the immature bone marrow-derived dendritic cells (DCs) leading to 57.3- and 13.3-fold higher production of interferon β and interleukin-6 than free cGAMP, respectively. The potent STING activation capacity is likely due to the efficient cellular internalization of MnP-PEG nanoclusters by DCs and acid-triggered release of Mn^{2+} ions in the endolysosomes. Intratumoral administration of MnP-PEG nanoclusters markedly enhances tumor infiltration as well as maturation of DCs and macrophages, and promotes activation and cytotoxicity of T cells and natural killer cells in the tumor. MnP-PEG nanocluster in combination with a checkpoint inhibitor leads to significant tumor regression in the B16F10 murine melanoma model without any overt toxicities.

1. Introduction

Stimulator of interferon genes (STING) pathway has emerged as a promising target for cancer immunotherapy. Activation of STING protein on the endoplasmic reticulum (ER) surface triggers the downstream signaling events via the recruitment and activation of TANK-binding kinase 1 (TBK1), interferon regulatory factor 3 (IRF3), and nuclear factor Kappa B (NF-κB),[1–3] which induce the expression and secretion of type I interferons (IFNs) and proinflammatory cytokines, such as IFN-β and interleukin-6 (IL-6).[4,5] Type I IFNs subsequently promote maturation and antigen presentation of dendritic cells (DCs) and thereby T cell priming orchestrating the innate and adaptive immunity against cancer. Therapeutic benefits of targeting STING pathway have been demonstrated in preclinical murine tumor models.[6–9] Several clinical trials are ongoing to assess the antitumor efficacy of STING agonists in mono- or combination therapies.[10]

Cyclic dinucleotides (CDNs) are natural STING agonists but the clinical application of CDNs as immunotherapeutics remains a significant challenge. Owing to the intrinsic properties of negative charge and small molecular weight, CDNs have poor cytosolic bioavailability and undesired pharmacokinetics in vivo.[11] In addition, they are highly susceptible toward enzymatic degradation primarily by ecto-necleotide pyrophosphatase phosphodiesterase 1 (ENPP1).[2] Ligands alternative to CDNs and nanoparticles or hydrogels carrying CDNs are being actively pursued in order to overcome these limitations for the clinical applications.[7,8,11–19] Despite these ongoing efforts, a facile therapeutic intervention that targets STING pathway is highly desired.

Manganese (Mn) is an essential trace element to human health, which is involved in many physiological processes including antitumor immune responses.[20–22] Recently, Mn^{2+} ions have been discovered to directly activate the cyclic GMP-AMP synthase (cGAS), the cytosolic DNA sensor, to synthesize 2′3′-cyclic GMP-AMP (referred as cGAMP for simplicity).[21,23] However, direct administration of Mn^{2+} ion in vivo results in insufficient accumulation of Mn^{2+} ions to reach an effective concentration in the tumor microenvironment[24] and the diffusion of Mn^{2+} ions

M. Gao, Y.-Q. Xie, Dr. Y. Zhao, Dr. S. Van Herck, Dr. Y. Guo, X. Hu, Prof. L. Tang
Institute of Bioengineering
École Polytechnique Fédérale de Lausanne (EPFL)
Lausanne 1015, Switzerland
E-mail: li.tang@epfl.ch

K. Lei, Dr. Y. Zhao, A. Kurum, Dr. Y. Guo, Prof. L. Tang
Institute of Materials Science and Engineering
École Polytechnique Fédérale de Lausanne (EPFL)
Lausanne 1015, Switzerland

The ORCID identification number(s) for the author(s) of this article can be found under https://doi.org/10.1002/adtp.202100065

DOI: 10.1002/adtp.202100065

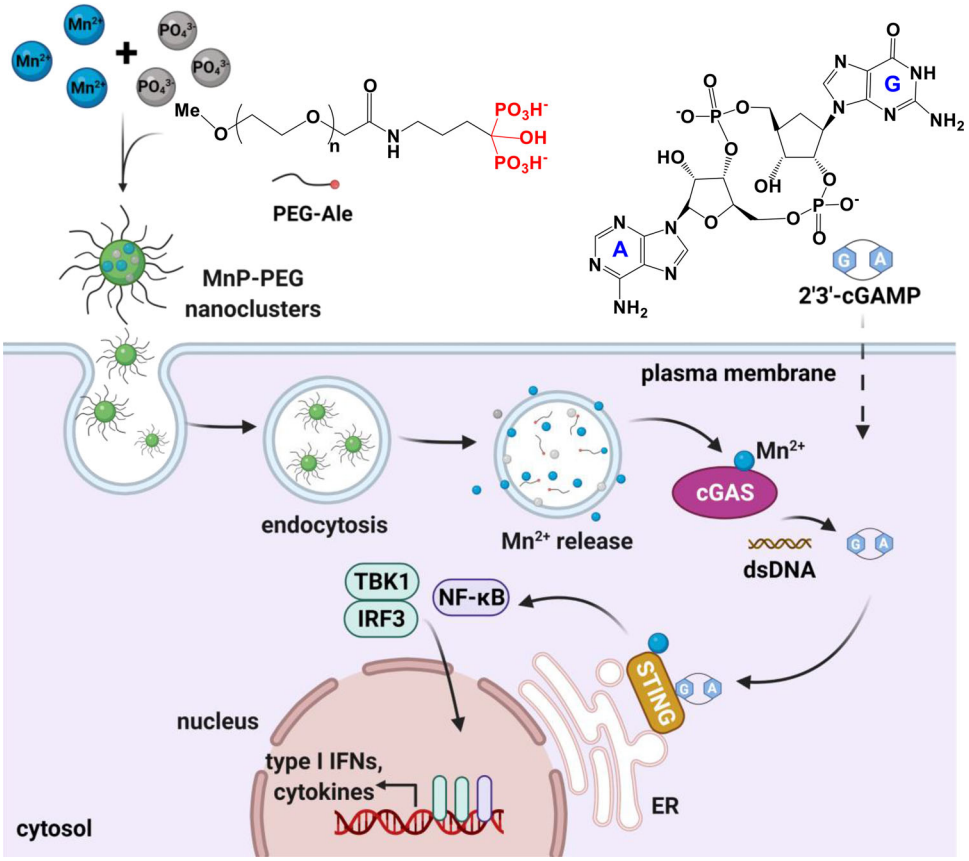

Figure 1. Schematic illustration of the synthesis and cGAS-STING activation mechanism of MnP-PEG nanoclusters. PEG-Ale, polyethylene glycol conjugated with a terminal alendronate; A, adenosine monophosphate; G, guanosine monophosphate; 2′3′-cGAMP, 2′3′-cyclic GMP-AMP; dsDNA, double-stranded DNA; ER, endoplasmic reticulum; TBK1, TANK binding kinase 1; IRF3, interferon regulatory factor 3; NF-κB, nuclear factor kappa B.

into other tissues, such as brain, leading to potential toxicity.[25] Here, we developed an Mn-based nanoparticulate STING agonist that could effectively activate the STING pathway in vitro and elicit robust anticancer immune responses in vivo (**Figure 1**). We prepared a polyethylene glycol (PEG)-modified manganese(II) phosphate nanocluster (MnP-PEG) using a facile coprecipitation method in solution at ambient temperature. MnP-PEG nanoclusters were efficiently internalized by DCs through endocytosis and subsequently released Mn^{2+} ions triggered by the acid condition in the endolysosomes leading to potent STING activation. MnP-PEG administered in vivo promoted infiltration and maturation of DCs and macrophages and augmented activation and granzyme B production of $CD8^+$ T cells and natural killer (NK) cells in the tumor microenvironment. When combined with a checkpoint blockade antibody, MnP-PEG synergistically boosted antitumor efficacies by inhibiting tumor progression in a mouse melanoma model.

2. Results and Discussion

We first sought to synthesize an Mn-loaded nanoparticle that is biocompatible and stay non-aggregated in physiological conditions. Inspired by the synthesis of calcium phosphate nanoparticles,[26,27] we fabricated manganese(II) phosphate (MnP) particles by mixing the Mn^{2+} and PO_4^{3-} ions in solution. The as obtained MnP particles were in micro-size and unstable (Figure S1, Supporting Information). In order to stabilize MnP particles, we added a phosphate-functionalized PEG (PEG-Ale) polymer[28] during the nanoparticle synthesis to obtain PEGylated MnP (MnP-PEG) (Figure 1; Figure S2, Supporting Information). MnP-PEG are nanoclusters with an average diameter of 150.0 ± 39.7 nm (**Figure 2**A,B). The successful PEGylation of MnP-PEG was evidenced by the shift of zeta-potential from positive to slightly negative (from 12.6 to −11.0 mV) (Figure 2C). MnP-PEG was stable and stayed non-aggregated in the phosphate-buffered saline (PBS) buffer for at least one week (Figure 2D). Analysis of scanning electron microscopy-energy dispersive X-ray (SEM-EDX) further confirmed the uniformed element distribution of Mn (49.2%), P (18.6%), and O (32.0%) in MnP-PEG nanoclusters (Figure 2E). Importantly, MnP-PEG exhibited good biocompatibility and low toxicities against B16F10 melanoma tumor cells even at high concentrations (Figure 2F).

We next assessed the STING activation capacity of MnP-PEG nanoclusters in vitro. Using the THP1-Dual reporter cell line,[29] a human monocytic cell line with a stably integrated IRF-inducible reporter construct, we showed that MnP-PEG nanoclusters induced luminescence signals in a dose-dependent manner. At a concentration of Mn^{2+} ions as low as 0.1 mM, MnP-PEG elicited as potent IFN-luciferase response as cGAMP

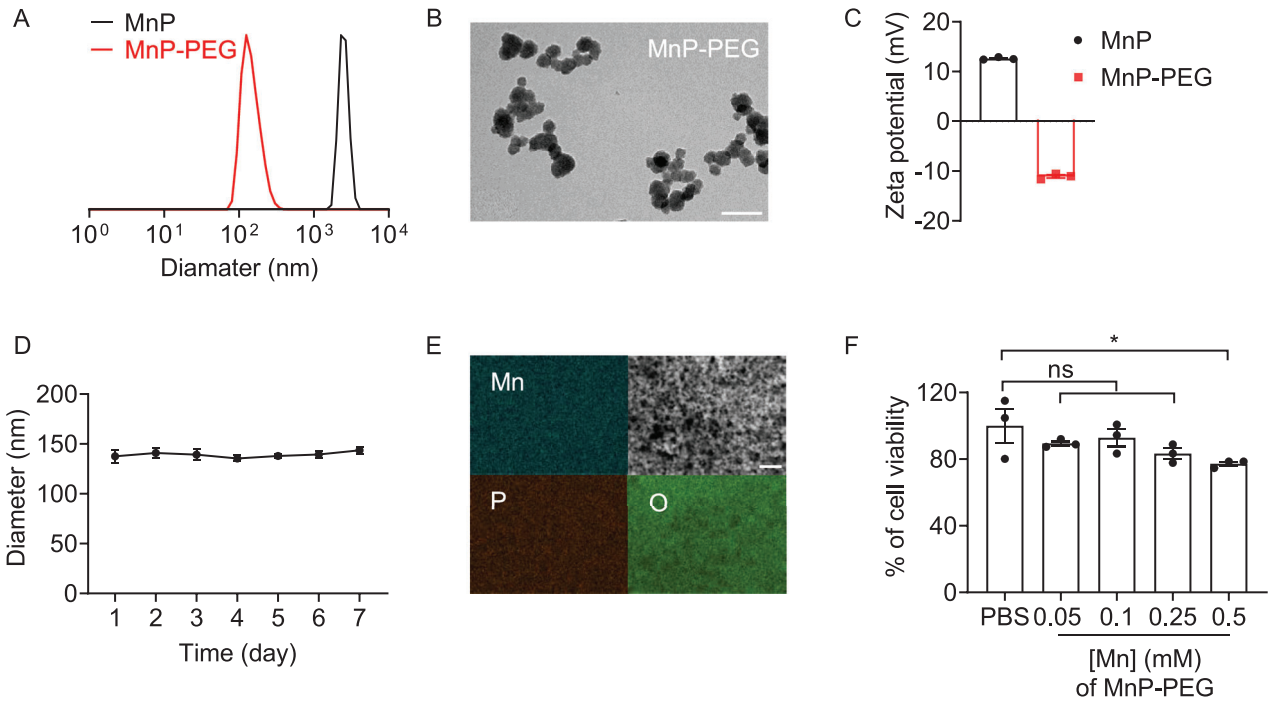

Figure 2. Characterizations of MnP-PEG nanoclusters. A) Dynamic light scattering results of MnP particles and MnP-PEG nanoclusters. B) TEM image of MnP-PEG nanoclusters. The scale bar is 100 nm. C) Zeta potentials of MnP particles and MnP-PEG nanoclusters. D) Size monitoring of MnP-PEG nanoclusters in the PBS solution (pH = 7.4) over time. E) SEM-EDX image of MnP-PEG nanoclusters. The scale bar is 500 nm. F) Percentages of cell viability of B16F10 cells incubated with MnP-PEG nanoclusters at different concentrations for 24 h. All data represent mean ± standard error of the mean (SEM) ($n = 3$), and are analyzed by one-way ANOVA and Tukey's test; *$p < 0.05$; ns, not significant.

(1.5 μM)[30–32] in a 24-hour incubation assay (**Figure 3**A), indicating that MnP-PEG nanoclusters could effectively activate the cGAS-STING pathway. Notably, treatment with MnP-PEG at concentrations below 0.75 mM showed minimal impact on the viability of THP1-Dual cells up to 24-hour incubation (Figure S3, Supporting Information). However, when the incubation time was extended to 48 h, more potent STING activation effect was observed along with higher cytotoxicity (Figure S4, Supporting Information). IFN-β is one kind of type I IFNs and an important indicator of the STING pathway activation. We further determined the IFN-β production in the DC2.4 dendritic cell line using the enzyme-linked immunosorbent assay (ELISA) (Figure 3B). Incubation of DC2.4 cells with MnP-PEG nanoclusters at a concentration of [Mn] = 0.5 and 0.25 mM induced significant secretion of IFN-β in the culture, which was 3.6- and 2.4-fold higher than that of soluble cGAMP, respectively. In addition, MnP-PEG nanoclusters ([Mn] = 0.25 mM) increased the mRNA levels of genes encoding pro-inflammatory cytokines, including *Ifnb1*, *Il6*, *Tnfa*, to a higher or comparable extent in comparison with cGAMP as measured by quantitative reverse transcription polymerase chain reaction (qRT-PCR) (Figure 3C–E). In line with the enhanced type I IFN and cytokine production, we found the treatment of MnP-PEG nanoclusters, but not the free cGAMP (1.5 μM), led to robust activation of DC2.4 cells as indicated by the markedly increased expression of maturation markers such as CD80, CD86, and major histocompatibility complex class II (MHC-II) (Figure 3F–H).

Next, we tested whether MnP-PEG could activate the STING pathway in primary DCs. We collected the immature bone marrow-derived dendritic cells (BMDCs) from C57BL/6 mice and cultured them in the presence of granulocyte-macrophage colony-stimulating factors (GM-CSF). In agreement with the results of DC2.4 cells, MnP-PEG treatment induced remarkable production of IFN-β and IL-6 at a similar dose-dependent manner (**Figure 4**A,B). BMDCs treated by MnP-PEG at the concentration of [Mn] = 0.5 mM secreted 57.3- and 13.3-fold higher amount of IFN-β and IL-6 than the free cGAMP, respectively. In addition, MnP-PEG treatment resulted in elevated expression of CD80, CD86, and MHC-II, suggesting that MnP-PEG induced maturation of BMDCs (Figure 4C–E). Besides DCs, we found MnP-PEG also activated the STING pathway in macrophages. When RAW264.7 murine macrophages were exposed to MnP-PEG nanoclusters, they produced a significant amount of IFN-β in a dose-dependent manner (Figure S5, Supporting Information). Similarly, the treatment of MnP-PEG nanoclusters promoted the expression of CD80, CD86, and MHC-II in RAW264.7 macrophages (Figure S6, Supporting Information), suggesting that MnP-PEG also induced macrophage maturation.

In order to understand how MnP-PEG could stimulate the cGAS-STING pathway, we incubated DC2.4 cells with fluorescently labeled MnP-PEG nanoclusters to investigate the cellular interactions (Figure S7, Supporting Information). MnP-PEG nanoclusters labeled with Alex Fluor 488 exhibited massive cellular internalization as evidenced by the measurement of mean fluorescent intensity (MFI) by flow cytometry (**Figure 5**A,B). The fluorescence intensity detected in DC2.4 cells treated with labeled

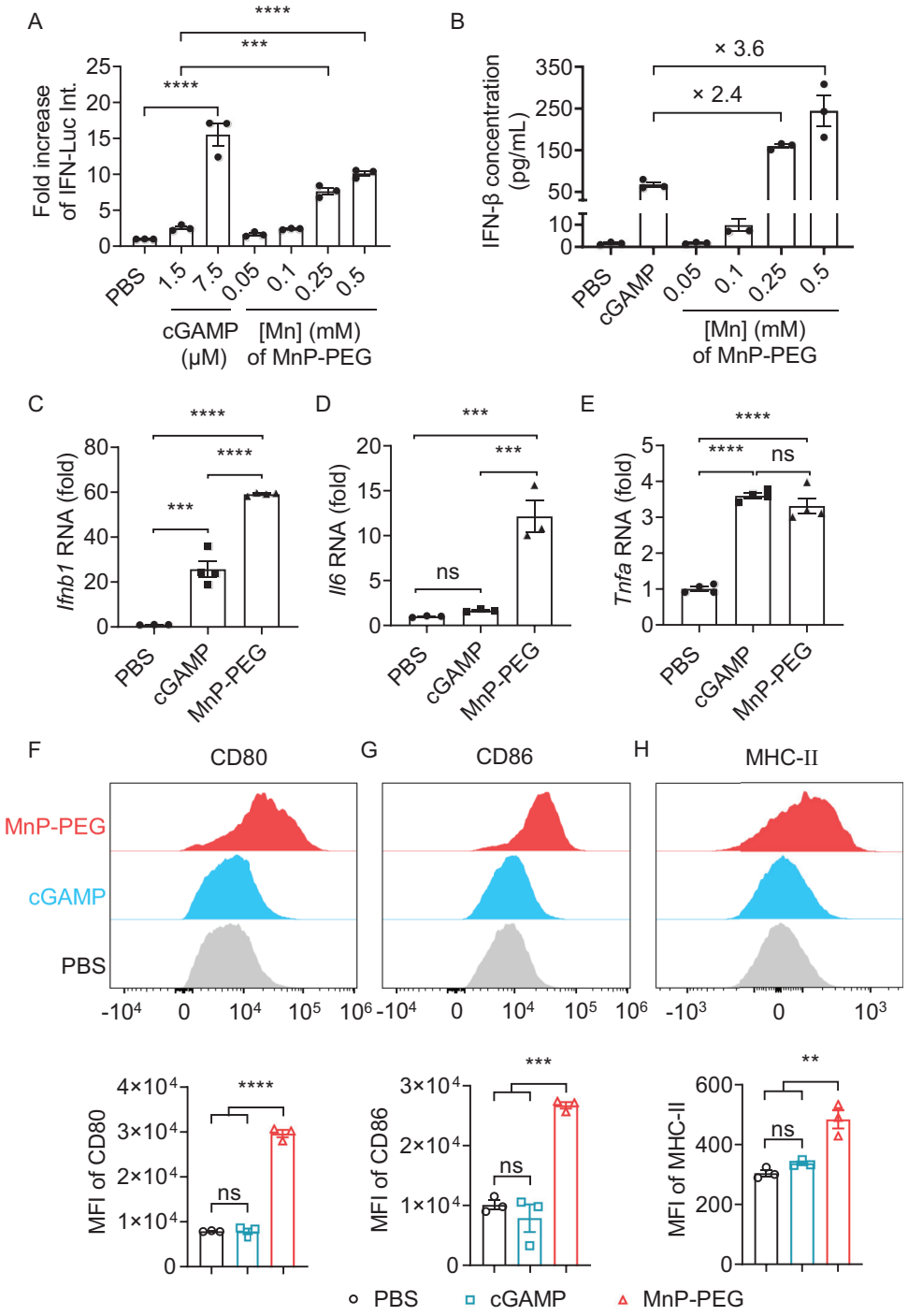

Figure 3. MnP-PEG nanoclusters activated the STING pathway in THP1-Dual and DC2.4 cells. A) Fold increase of IFN-induced luminescence signals (IFN-Luc Int.) in THP1-Dual cells incubated with cGAMP (1.5 and 7.5 μM) or MnP-PEG nanoclusters at different concentrations for 24 h as compared to that of PBS control. B) IFN-β levels in the supernatant of DC2.4 cells incubated with cGAMP (1.5 μM) or MnP-PEG nanoclusters at different concentrations for 24 h. C–E) RT-qPCR analysis of mRNA expression of *Ifnb1*, *Il6*, and *Tnfa* in DC2.4 cells incubated with cGAMP (1.5 μM) or MnP-PEG nanoclusters ([Mn] = 0.25 mM) for 24 h. F–H) Flow cytometry analysis and quantification of mean florescence intensity (MFI) of maturation markers (CD80, CD86, MHC-II) on DC2.4 cells incubated with cGAMP (1.5 μM) or MnP-PEG nanoclusters ([Mn] = 0.25 mM) for 24 h. All data represent mean ± SEM ($n = 3$), and are analyzed by one-way ANOVA and Tukey's test, ** $p < 0.01$, *** $p < 0.001$, **** $p < 0.0001$; ns, not significant.

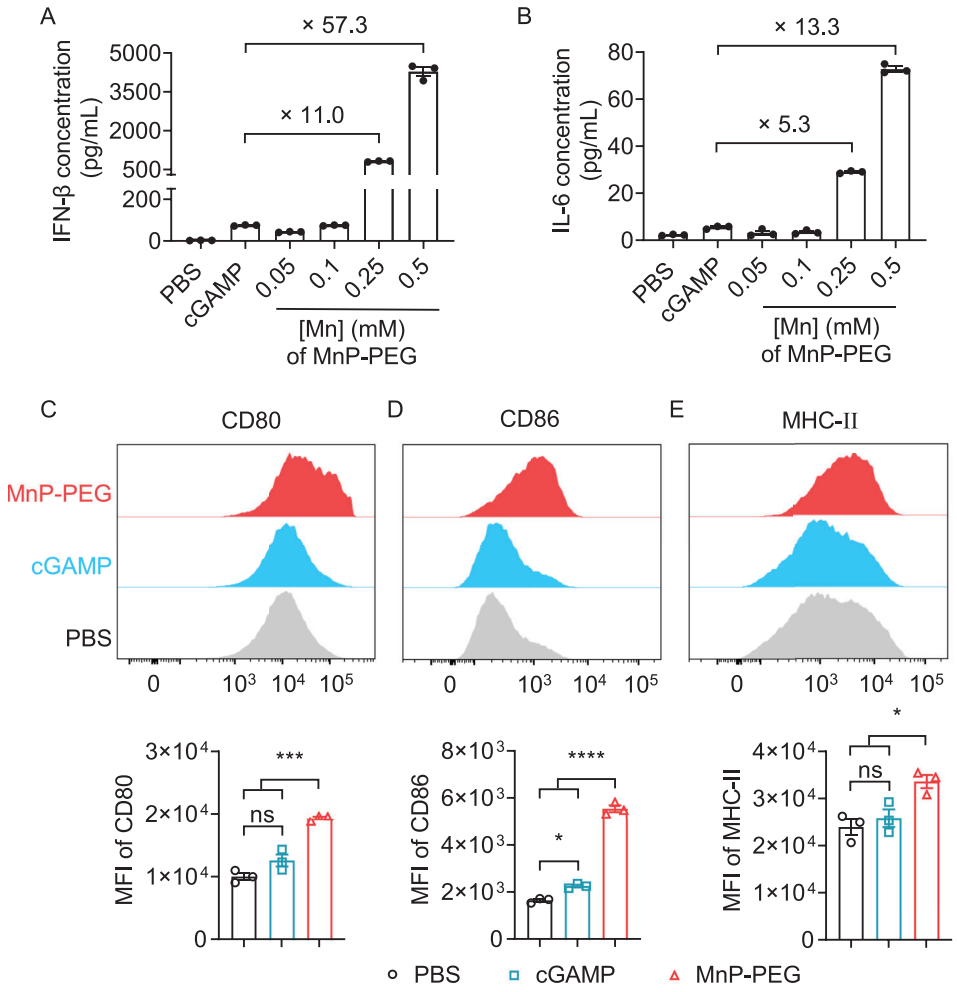

Figure 4. MnP-PEG nanoclusters activated the STING pathway in BMDCs. A,B) IFN-β and IL-6 levels in the supernatant of BMDCs incubated with cGAMP (1.5 μM) or MnP-PEG nanoclusters at different concentrations for 24 h. C–E) Flow cytometry analysis and quantification of MFI of maturation markers (CD80, CD86, MHC-II) on BMDCs incubated with cGAMP (1.5 μM) or MnP-PEG nanoclusters ([Mn] = 0.25 mM) for 24 h. All data represent mean ± SEM ($n = 3$), and are analyzed by one-way ANOVA and Tukey's test, $^*p < 0.05$, $^{***}p < 0.001$, $^{****}p < 0.0001$; ns, not significant.

MnP-PEG nanoclusters was 76.8-fold higher than that of cGAMP with the equivalent fluorescent labeling. cGAMP showed low cell membrane permeability and cellular internalization likely due to the negative charges. We further confirmed the cellular internalization and investigated the intracellular distribution of MnP-PEG nanoclusters with confocal laser scanning microscopy (CLSM). The CLSM images showed that MnP-PEG nanoclusters were internalized by cells through endocytosis and co-localized with endolysosomes (Figure 5C). The amount of internalized MnP-PEG nanoclusters by DC2.4 cells increased over time (Figure S8, Supporting Information). Due to the acidic environment inside the endolysosomes,[14] we speculated that MnP-PEG would release Mn^{2+} ions, which subsequently entered the cytosol and activated the cGAS-STING pathway. To mimic the acidic condition of lysosomes, MnP-PEG nanoclusters were exposed to an acid solution (pH 5.4), in which the average diameter decreased from 150 nm to ≤5 nm within 24 h indicating the quick dissolution of the nanoclusters (Figure 5D). In addition, we measured the released Mn^{2+} ions using inductively coupled plasma mass spectrometry (ICP-MS). MnP-PEG nanoclusters in acidic condition released 19.8% of Mn^{2+} ions within 24 h (Figure 5E).

Encouraged by the in vitro results showing enhanced STING activation capacity of MnP-PEG nanoclusters, we next examined whether MnP-PEG could activate immune cells in vivo. C57BL/6 mice bearing B16F10 tumors were intratumorally injected with MnP-PEG nanoclusters and sacrificed for flow cytometry analysis of tumor infiltrating immune cells (**Figure 6**A). Treatment of MnP-PEG nanoclusters markedly promoted tumor infiltration of DCs and macrophages (Figure 6B,C). In particular, the counts of intratumoral plasmacytoid DCs (pDC, defined as $CD11c^+Siglec\text{-}H^{high}$), which have been reported as the principal type I IFN-producing cells,[33] were increased 7.2-fold as compared to the non-treatment control (Figure S9A, Supporting Information). In addition, the expression of CD86 on DCs as well as CD80, CD86, and MHC-II on pDCs were significantly upregulated (Figure 6D; Figure S9B–D, Supporting Information), suggesting that MnP-PEG nanoclusters induced significant DC maturation in the tumor microenvironment. Upon activation of STING pathway in

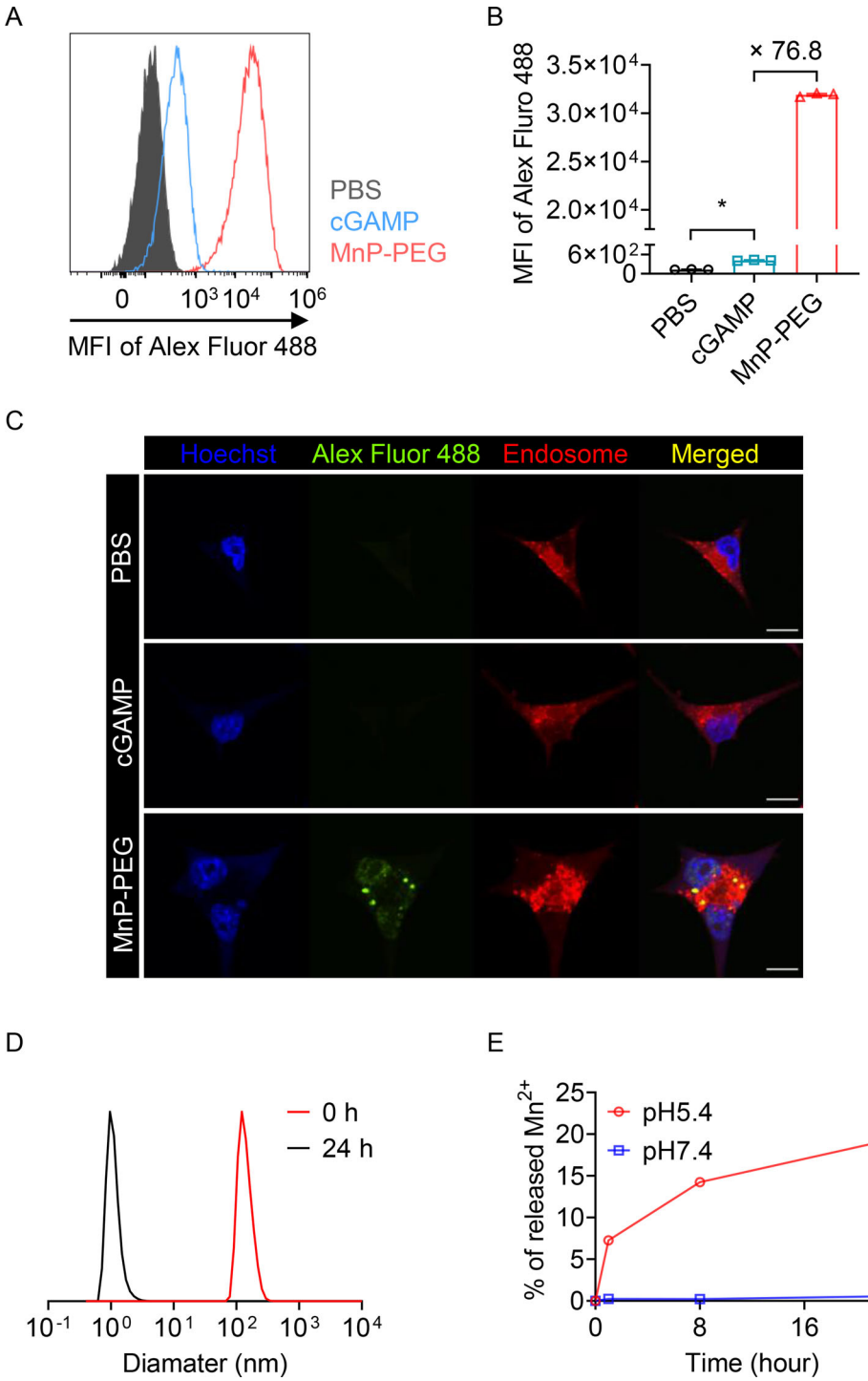

Figure 5. MnP-PEG nanoclusters were endocytosed by DC2.4 cells and released Mn^{2+} ions in response to acidic pH. A,B) Representative histograms and MFI of DC2.4 cells incubated with PBS, Alex Fluor 488-labeled cGAMP, or MnP-PEG nanoclusters for 2 h as analyzed by flow cytometry. C) Confocal laser scanning microscopy images of DC2.4 cells incubated with PBS, Alex Fluor 488-labeled cGAMP, or MnP-PEG nanoclusters for 2 h. The scale bar is 5 μm. D) Size monitoring of MnP-PEG in the PBS (pH 5.4) solution by dynamic light scattering. E) pH-responsive cumulative release of Mn^{2+} ions from MnP-PEG nanoclusters. All data represent mean ± SEM ($n = 3$), and are analyzed by one-way ANOVA and Tukey's test, $^*p < 0.05$.

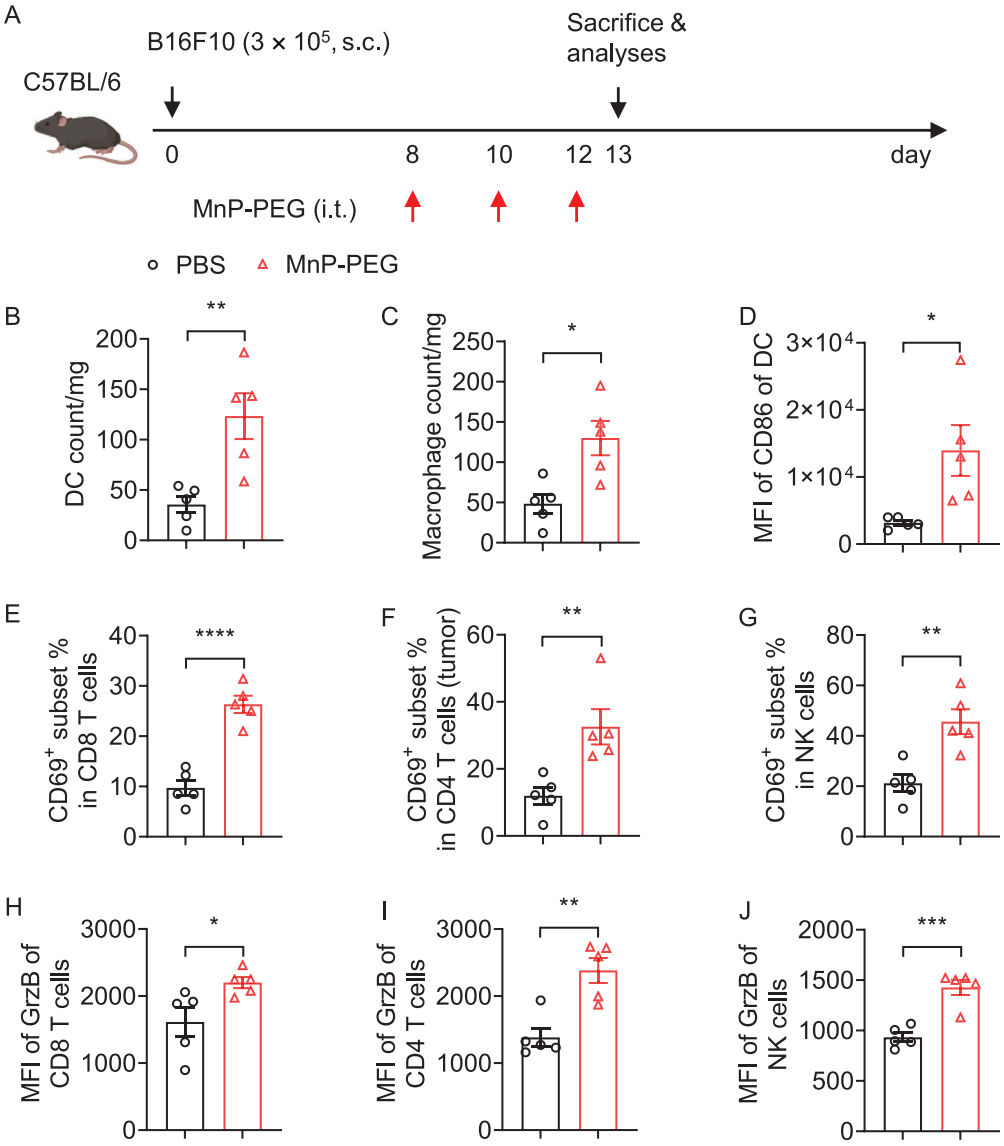

Figure 6. MnP-PEG nanoclusters remodeled the tumor immune microenvironment. A) C57BL/6 mice bearing subcutaneous (s.c.) B16F10 melanoma tumors were treated intratumorally (i.t.) with PBS or MnP-PEG for 3 doses and sacrificed for flow cytometry analysis of tumor-infiltrating immune cells. B,C) Counts of DCs and macrophages. D) MFI of CD86 on DCs. Percentages of $CD69^+$ subset among E) $CD8^+$ T cells, F) $CD4^+$ T cells, and G) NK cells. MFI of granzyme B (GrzB) production in H) $CD8^+$ T cells, I) $CD4^+$ T cells, and J) NK cells. All data represent mean ± SEM ($n = 5$), and are analyzed by two-sided Student's *t*-test, $^*p < 0.05$, $^{**}p < 0.01$, $^{***}p < 0.001$, $^{****}p < 0.0001$.

DCs and macrophages by MnP-PEG nanoclusters, the secreted type-I IFNs and proinflammatory cytokines could further prime the cytotoxic lymphocytes. Indeed, the frequencies of activated ($CD69^+$) tumor-infiltrating $CD8^+$ and $CD4^+$ T cells and NK cells were significantly increased (Figure 6E–G). Furthermore, the production of granzyme B by $CD8^+$, $CD4^+$ T cells, and NK cells was greatly enhanced, suggesting that the treatment of MnP-PEG nanoclusters promoted the cytotoxicity of tumor-infiltrating lymphocytes (Figure 6H–J).[34]

The markedly enhanced in vivo activation of DCs and tumor-infiltrating lymphocytes by MnP-PEG nanoclusters motivated us to evaluate its antitumor efficacy. In a therapeutic experiment setting, C57BL/6 mice were first inoculated with B16F10 cells (2×10^5), a murine melanoma model that is poorly immunogenic, followed by multiple injections of MnP-PEG (intratumoral [i.t.]), anti-PD-1 antibody (intraperitoneal [i.p.]) or the combination of these two every other day (**Figure 7**A). The treatment of MnP-PEG nanoclusters alone led to enhanced capacity in inhibiting tumor growth compared to the anti-PD-1 antibody treatment during the first 12 days but failed to control the tumor growth later (Figure 7B,C). The combination therapy of MnP-PEG nanoclusters and anti-PD-1 antibody induced synergistic therapeutic effect

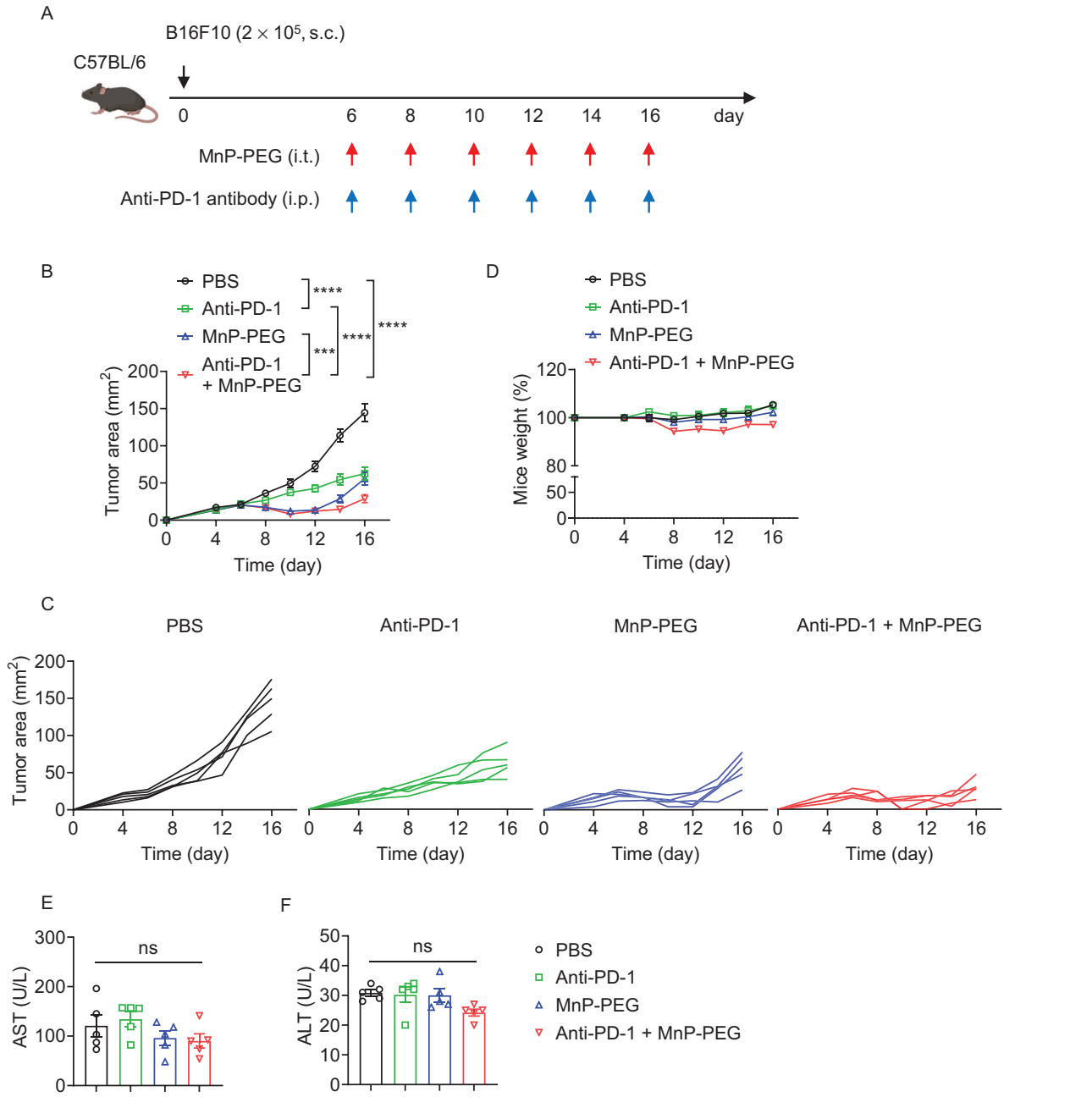

Figure 7. MnP-PEG nanoclusters induced antitumor efficacy in mono- or combination therapies. A) C57BL/6 mice bearing s.c. B16F10 melanoma tumors were treated starting from day 6 with PBS (i.t.), anti-PD-1 antibody (i.p.), MnP-PEG (i.t.), or the combination of antibody (i.p.) and MnP-PEG (i.t.) every two days for 6 doses. B) Tumor growth curves. Data are analyzed by two-way ANOVA and Tukey's test (shown are results of day 16). C) Individual tumor growth curves. D) Relative body weight of treated mice. E,F) Serum levels of aspartate aminotransferase (AST) and alanine transaminase (ALT). All data represent mean ± SEM ($n = 5$), and are analyzed by one-way ANOVA and Tukey's test, ***$p < 0.001$, ****$p < 0.0001$; ns, not significant; i.p., intraperitoneal.

with significant tumor regression (Figure 7B,C). Notably, either MnP-PEG nanoclusters alone or the combination of MnP-PEG nanoclusters and anti-PD-1 antibody exhibited no acute toxicity as all the treated mice showed no loss of body weight or elevation of serum levels of liver enzymes (Figure 7D–F). The high safety profile of Mn-based STING agonist observed here was consistent with the previously reported results.[22]

3. Conclusion

In summary, we developed a biocompatible MnP-PEG nanocluster that effectively stimulated the cGAS-STING pathway in vitro and in vivo leading to potent antitumor immune responses. The MnP-PEG nanoclusters were efficiently endocytosed by DCs and rapidly released a large number of Mn^{2+} ions in response to the

acidic environment in the endolysosomes. The intracellularly released Mn^{2+} ions have dual functions according to previous reports, 1) to directly activate the cytosolic DNA sensor, cGAS, to synthesize cGAMP,[23] and 2) to augment cGAMP-STING binding affinity.[21] Therefore, MnP-PEG nanoclusters exhibited potent cGAS-STING stimulating capacity.

As a non-nucleotidyl, nanoparticulate STING agonist, MnP-PEG nanocluster possesses several advantages as compared to natural CDNs, which could potentiate their future clinical applications. Slightly negatively charged surface (zeta potential −11.0 mV) as well as the suitable nanosize (diameter around 150.0 nm) of MnP-PEG nanoclusters render them potentially improved pharmacokinetics and enhanced retention in the tumor. MnP-PEG nanoclusters are resistant to enzymatic degradation and show good stability in buffers mimicking physiological conditions. The synthesis of MnP-PEG nanoclusters is a facile, scalable, and solution-based method, which might be compatible with large scale manufacturing process. We also found the MnP-PEG nanoclusters had excellent biocompatibility in vitro and in vivo. As Mn is an essential trace element to human health,[20,21] we anticipate that the Mn-based STING agonists might have good safety profiles for the clinical use.

Direct administration of free Mn^{2+} ions in vivo is in general much less effective as a therapeutic intervention because Mn^{2+} ions do not retain in the tumor microenvironment. In addition, the abundant PO_4^{3-} and CO_3^{2-} ions in the physiological condition may form Mn-consisting particles in situ with the injected Mn^{2+} ions (Figure S10, Supporting Information).[35,36] The randomly formed Mn-based particles in vivo may cause undesired variation and unexpected side effects, such as autoimmune responses, complexing the clinical results. To facilitate efficient tumor delivery of Mn^{2+} ions, nanoparticle and hydrogel based delivery systems have been developed as recently reported in several elegant studies.[24,37,38] The MnP-PEG nanocluster described here has well characterized physicochemical properties and does not require any additional chemotherapy or radiotherapy to generate intracellular double-stranded DNA for activation of the cGAS-STING pathway, and, therefore, represents a simple yet potent nanoparticulate STING activator.

4. Experimental Section

Materials: Manganese chloride ($MnCl_2$), disodium hydrogen phosphate (Na_2HPO_4), sodium chloride (NaCl), alendronate sodium trihydrate (Ale), sodium hydroxide (NaOH), 2-mercaptoethanol, bovine serum albumin (BSA), dimethyl sulfoxide (DMSO), and paraformaldehyde (PFA) were purchased from Sigma-Aldrich (St. Louis, MO, USA). Methoxy-PEG succinimidyl carboxymethyl ester (mPEG-NHS, $M_n \approx 5000$ Da) was purchased from JenKem Technology (Plano, TX, USA). Alexa Fluor 488 *N*-hydroxysuccinimide (NHS) ester, trihydrochloride (Hoechst 33342), Aqua live/dead stain, and Cell Activation Cocktail were purchased from Invitrogen (Carlsbad, CA, USA). Reagents for cell culture, including phosphate buffered saline (PBS), fetal bovine serum (FBS), high glucose Dulbecco's modified Eagle's medium (DMEM), Roswell Park Memorial Institute (RPMI) 1640 medium, trypsin solution, penicillin/streptomycin, HEPES, L-glutamine, 3-(4,5-dimethylthiazol-2-yl)-2,5-diphenyltetrazolium (MTT), and other experimental related reagents, such as Maxima SYBR Green Master Mix, 4′,6-diamidino-2-phenylindole (DAPI), IL-6 mouse ELISA kit, and ACK lysing buffer were purchased from Thermo Fisher Scientific (Waltham, MA, USA). Murine granulocyte-macrophage colony-stimulating factor (GM-CSF) was purchased from PeproTech (London, UK). ProLong diamond antifade mountant, LysoTracker Red DND-99, Cyto-Fast Fix/Perm Buffer, and all antibodies for flow cytometry analysis were purchased from Biolegend (San Diego, CA, USA). Cyclic guanosine monophosphate–adenosine monophosphate (cGAMP), QUANTI-Luc, Normocin and Lumikin Xpress mIFN-β 2.0 were purchased from InvivoGen (San Diego, CA, USA). cGAMP (Alex Fluor-488) was purchased from BioLog GmbH (Büttelborn, Germany). The Stanbio Chemistry Reagents were purchased from Stanbio Laboratory (Boerne, TX, USA). The anti-PD-1 antibody (Clone: 29F.1A12) was purchased from BioXcell (West Lebanon, NH, USA). Unless otherwise noted, all chemical and biological reagents were used as received.

Mice and Cell Lines: All mouse experimental procedures have been approved by the Swiss authorities (Canton of Vaud, animal protocol ID 3206 and 3533) and performed in accordance with the guidelines from EPFL CPG facility. Six to eight-week-old female C57BL/6 mice were purchased from Charles River Laboratories (Lyon, France) and maintained in the UDP animal facility. The THP1-Dual cell, a reporter cell line for NK-κB and IRF, was originally acquired from InvivoGen. The DC2.4 mouse dendritic cell line was a kind gift from Dr. K. L. Rock (Dana-Farber Cancer Institute). B16F10 murine melanoma cells and RAW264.7 cells were originally acquired from the American Type Culture Collection (ATCC, Manassas, VA, USA). THP1-Dual cells were cultured in RMPI 1640, supplemented with FBS (10%, v/v), penicillin/streptomycin (1%, v/v), L-glutamine (2 mM), HEPES (25 mM), and Normocin (100 μg mL^{-1}). The DC2.4 cells were cultured in in RMPI 1640, supplemented with FBS (10%, v/v), penicillin/streptomycin (1%, v/v), and L-glutamine (2 mM). B16F10 were cultured in DMEM, supplemented with FBS (10%, v/v) and penicillin/streptomycin (1%, v/v). RAW264.7 cells were cultured in DMEM, supplemented with FBS (10%, v/v) and penicillin/streptomycin (1%, v/v). Immature bone marrow-derived dendritic cells (BMDCs) were isolated from C57BL/6 mice (Charles River laboratory, Wilmington, MA, USA), and cultured in RPMI 1640 complete medium containing HI-FBS (10%, v/v), penicillin/streptomycin (1%, v/v), L-glutamine (2 mM), and 2-mercaptoethanol (50 μM) with GM-CSF (20 ng mL^{-1}) for 6 days at 37 °C with CO_2 (5%) before use.

Instrument: Nuclear magnetic resonance (NMR) spectra were acquired on a Bruker AVANCE NEO 400 MHz spectrometer (Billerica, MA, USA). The size and surface charge of MnP-PEG and MnP were measured by dynamic light scattering (DLS) on a Malvern NanoZS (Worcester, UK). The transmission electron microscopy (TEM) images was taken by FEI Tecnail Osiris TEM instrument (200 kV, Hillsboro, OR, USA) equipped with 4k × 2.6k Gatan Orius CCD camera. The scanning electron microscopy-energy dispersive X-ray analysis (SEM-EDX) images were performed on the GeminiSEM 300 (Jena, Germany) with Oxford instrument X-MAX detector for EDX analysis. The concentration of Mn of MnP-PEG was measured by inductively coupled plasma mass spectrometry (ICP-MS, Nexlon 350, PerkinElmer). The quantitative real-time PCR (qRT-PCR) was performed on QuantStudio 6 instrument (Applied Biosystems, USA). The fluorescence intensity of labelled samples was measured with a Varioskan Lux microplate reader (Thermo Fisher Scientific). The confocal laser scanning microscopy (CLSM) images were visualized via the Visitron Spinning Disk CSU W1 (Puchheim, Germany). All the flow cytometry data were acquired using an Attune NxT flow cytometer (Thermo Fisher Scientific). And the data processing of flow cytometry was performed with FlowJo software (BD, Ashland, USA)

Synthesis of PEG-Ale and Alex Fluor 488-Ale: PEG-Ale was synthetized according to a reported method with minor modification.[28] Ale (400 mg, 1.23 mmol) was dissolved in NaOH solution (2 N, 1 mL), followed by adding ultrapure H_2O (800 μL, 18.2 MΩ cm). The pH value of the solution was adjusted to 7 by dropwise addition of HCl (1 N). mPEG-NHS (75 mg, 13.8 μmol) was dissolved in ultrapure H_2O (400 μL) and then dropwise added to the Ale solution under vigorous stirring. The reaction mixture was stirred at 4 °C for 1 h, followed by overnight stirring at room temperature. The compound was purified by dialysis (MWCO = 3000 Da) with ultrapure H_2O. Finally, the obtained solution was freeze-dried to get PEG-Ale. The PEG-Ale was characterized by ^{1}H NMR. Ale: ^{1}H NMR (400 MHz, Deuterium Oxide) δ ppm: 3.12–2.99 (m, 2H, NH_2—CH_2), 2.10–1.94 (m, 4H, CH_2—CH_2—C). PEG-Alendronate: ^{1}H NMR (400 MHz, Deuterium

Oxide) δ ppm: 4.22 (s, 2H, O—CH_2—CONH), 3.72 (s, 636H, PEG), 3.39 (s, 4H, CH_3—O—), 3.17 (t, J = 6.7 Hz, 2H, CONH—CH_2—), 1.99 (q, J = 14.9, 13.8 Hz, 2H, CH_2—CH_2—C), 1.83 (d, J = 7.9 Hz, 2H, CH_2—CH_2—C).

To synthesize Alex Fluor 488-Ale, Alex Fluor 488-NHS (54 µg, 138 nmol) instead of mPEG-NHS was added to the Ale solution (4 mg, 12.3 µmol) following the same procedure. The mixture was used for the next step without purification.

Preparation of MnP-PEG Nanoclusters: Follow the synthesis of calcium phosphate nanoparticles, manganese phosphate system was developed. Briefly, HEPES buffer (50 mM, 400 µL) containing NaCl (140 mM) and Na_2HPO_4 (1.5 mM) was mixed with a $MnCl_2$ solution (250 mM, 400 µL) under vigorous stirring. After particle nucleation, a solution of PEG-Ale (200 µM, 400 µL) in ultrapure H_2O was quickly added to stabilize the MnP particles. The mixture was shaken (1000 rpm) for 1 h at 25 °C followed by centrifugation at 14 800 rpm for 5 min. The pellet was dispersed in PBS (100 µL) after discarding the supernatant. For MnP particles without PEG modification, PEG-Ale was not added. For dye labeled MnP-PEG (Alex-MnP-PEG), a solution (400 µL) of Alex Fluor 488-Ale (30 µM) and PEG-Ale (200 µM) in ultrapure H_2O was added to modify the MnP.

Characterizations of MnP-PEG Nanoclusters: The size distribution and Zeta potentials of MnP, MnP-PEG were analyzed by DLS at 25 °C. TEM was used to characterize the morphology of MnP and MnP-PEG nanoclusters. SEM-EDX was applied to qualitatively analyze the different element distributions among MnP-PEG nanoclusters. The stability of MnP-PEG in the PBS solution was assessed by monitoring changes in size for one week, and the size was determined by DLS.

MTT Assay: To study the in vitro cellular toxicity of MnP-PEG nanoclusters, the MTT assay was performed according to the standard protocol. B16F10 cells (10k cells $well^{-1}$, 100 µL) were seeded in a 96-well plate overnight. MnP-PEG nanoclusters and 2'3'-cGAMP (referred as cGAMP for simplicity) were added into wells with different concentrations. After 24 or 48 h incubation, the culture medium was discarded and MTT solution (0.5 mg mL^{-1}, 100 µL) was added, followed by further incubation for 4 h. Then the MTT solution was trashed and DMSO (100 µL) was added. The plate was shaken on an orbital shaker at 500 rpm for 15 min and then the absorbance of each well was read at OD = 590 nm.

Stimulation of STING Pathway in THP1-Dual Reporter Cells: THP1-Dual cell suspension (100k cells $well^{-1}$, 180 µL) was plated into a flat-bottom 96-well plate. MnP-PEG nanoclusters with different concentrations ([Mn] = 0.05, 0.1, 0.25, 0.5 mM), free cGAMP (1.5 and 7.5 µM) and PBS were added into set wells. Incubated for 24 h, THP1-Dual cell culture medium (20 µL) was pipetted from each well into a 96-well white plate. A QUANTI-Luc assay solution (50 µL) was added into each well of the 96-well white plate for luminescence signal measurement (0.1 s reading time). In addition, all cells were resuspended with DAPI buffer for cell viability test using flow cytometry.

Stimulation of STING Pathway in DC2.4 and RAW264.7 Cells Lines, and BMDCs: DC2.4 cells were plated into a 24-well plate (0.5 M cells $well^{-1}$, 0.5 mL) and incubated with MnP-PEG nanoclusters ([Mn] = 0.05, 0.1, 0.25, 0.5 mM), free cGAMP (1.5 µM), and PBS for 24 h. All DC2.4 cells then were harvested for FACS analyses. The supernatant was collected for ELISA tests to measure the concentrations of IFN-β and IL-6 using Lumikin Xpress mIFN-β 2.0 and IL-6 ELISA kit, respectively. Similar studies were performed with RAW264.7 macrophages and BMDCs.

qRT–PCR Assay: Total RNA was extracted from DC2.4 cells, which had been incubated with MnP-PEG nanoclusters ([Mn] = 0.25 mM), cGAMP (1.5 µM) and PBS for 24 h. Total RNA was isolated using the RNAeasy Mini Kit following the manufacturer's instructions, and cDNA was synthesized with the SuperScript III Reverse Transcriptase, RNasin Plus RNase Inhibitor in the presence of random primers and the Deoxynucleoside Triphosphate Set. Quantitative RT-PCR was performed in quadruplicates using Maxima SYBR Green Master Mix on the QuantStudio 6 qPCR instrument. The data were invariably normalized to the expression levels of β-actin. The following primers were used for qRT–PCR.

β-actin: TCCAGCCTTTCTTGGT; GCACTGTGTTGGCATAGAGGTC
Ifnb1:[23] CACAGCCCTCTCCATCAACT; TCCCACGTCAATCTTTCCTC
Il6:[39] ATCCAGTTGCCTTCTTGGGACTGA; TAAGCCTCCGACTTGTGAAGTGGT
Tnfa:[40] CTGTAGCCCACGTCGTAGC; GGTTGTCTTTGAGATCCATGC

Cellular Internalization Assay: The in vitro cellular uptake of MnP-PEG nanoclusters in immune cells was tested by the flow cytometry. DC2.4 cells (2×10^5 cells per well, 0.5 mL) were plated into a 24-well plate overnight. Then MnP-PEG and soluble cGAMP containing the equivalent amounts of tagged Alex Fluor 488 were added into each designed well for further 6-h incubation. All cells of each well were harvested and washed three times with a PBS solution containing 0.2%/w/v BSA (termed FACS buffer) to remove free MnP-PEG or cGAMP. Finally, the DC2.4 cells were resuspended with the DAPI solution (0.1 µg mL^{-1}, 150 µL) for flow cytometry analyses.

Confocal Fluorescence Imaging: Then Confocal fluorescent microscope was applied to observe the intracellular distribution of MnP-PEG nanoclusters within immune cells. DC2.4 cells (2×10^5 cells per well, 0.5 mL) were plated on the surface of round glass coverslips, which had been put into the wells of a 24-well plate. After overnight incubation, MnP-PEG and soluble cGAMP containing the equivalent amounts of Alex Fluro 488 were added into each designed well for further two hour's incubation. At set time points, the DC2.4 cells were washed with PBS (1 mL) for twice and then stained with LysoTracker Red DND-99 (125 nM) and Hoechst 33342 (4 µM) in serum-free RPMI-1640 medium (0.5 mL) for 2 h in the incubator, separately for endo/lysosome and nuclei staining, followed by twice PBS washing (1 mL). DC2.4 cells were then fixed with PFA (4%, 200 µL) for 10 min, washed by PBS (1 mL) for twice. Then the coverslips were gently coated over a glass slide with ProLong diamond antifade mountant (10 µL). The DC2.4 cells were imaged with Confocal microscope with a 60 × Oil Objective.

Release Kinetics of Mn^{2+} at Neutral or Acidic pH: The pH-responsive release profile of Mn^{2+} ions from MnP-PEG nanoclusters was analyzed with DLS and ICP-MS. Briefly, MnP-PEG nanoclusters (1 mg) were resuspended in PBS (1 mL) buffer with different pH values (5.4 and 7.4) under shake (1000 rpm). In 24 h, the size shift of MnP-PEG nanoclusters under different conditions were tested. Meanwhile, at set time points (1, 8, 24 h), MnP-PEG based solutions (50 µL) were centrifuged and the supernatants were collected for ICP-MS test, and the release efficiencies were calculated as follows.

$$\%\ \text{of release ions} = \text{weight of manganese released from MnP-PEG nanoclusters} / \text{total weight of manganese in MnP-PEG nanoclusters} \times 100\% \quad (1)$$

Flow Cytometry Analyses of Tumor Infiltrating Immune Cells: Female C57BL/6 mice, 6–8 weeks in age, were subcutaneously inoculated with B16F10 mouse melanoma cells (3×10^5) on the right-side flank. On day 8, mice were treated with PBS (intratumoral injection [i.t.], 50 µL) or MnP-PEG (i.t., [Mn] = 13 mM, 50 µL) every two days for three doses in total. All mice were euthanized on day 13 to collect tumors tissues. The collected tumors were cut into pieces with a scissor and treated with dissociation buffer (2 mL) under shaking (1000 rpm) at 37 °C for 1 h. Red blood cells were lysed with ACK lysing buffer at room temperature for 5 min. All cells were stained with corresponding surface markers, followed by the Aqua live/dead staining at 4 °C for 20 min. For the intracellular staining, cells were pretreated with Cell Activation Cocktail at 37 °C for 4 h. Then cells were fixed and permeabilized with the Cyto-Fast Fix/Perm Buffer and stained with anti-cytokine antibodies. Finally, cells were resuspended in the FACS buffer for flow cytometry analyses.

Antitumor Efficacy Study: Female C57BL/6 mice, 6–8 weeks in age, were subcutaneously inoculated with B16F10 mouse melanoma cells (2×10^5) on the right-side flank. Mice were treated with PBS (i.t.), anti-PD-1 antibody (intraperitoneal, i.p., 2 mg mL^{-1}, 100 µL), MnP-PEG nanoclusters (i.t., [Mn] = 13 mM, 50 µL), or the combination of anti-PD-1 antibody and MnP-PEG nanoclusters every two days starting from day 6 until day 16. Tumor area and body weight were monitored every two days. Tumor

area was calculated according to the formula, area = length × width (the length and width of tumors were measured by digital calipers).

Serum Levels of Liver Enzymes: Serum samples were collected for analyses when mice were sacrificed on day 13 (same experimental setting as in the section "Flow cytometry analyses of tumor infiltrating immune cells"). The serum levels of alanine transaminase (ALT) and aspartate transaminase (AST) in serum were measured using Stanbio Chemistry Reagents per the manufacturer's instructions.

Statistical Analysis: Statistical analysis was processed through GraphPad Prism 9 (GraphPad software, Inc., La Jolla, CA, USA). Unless otherwise noted, the data were presented as mean ± standard error of the mean (SEM). Sample sizes and methods for statistical analysis were indicated in figure captions. Comparisons of two groups were performed by using two-tailed unpaired Student's *t*-test. Comparisons of multiple groups at a single time point were performed by using one-way or two-way analysis of variance (ANOVA) and Tukey's test. p values are presented as $*p < 0.05$, $**p < 0.01$, $***p < 0.001$, $****p < 0.0001$. No statistically significant (ns) differences were considered when $p > 0.05$.

Supporting Information

Supporting Information is available from the Wiley Online Library or from the author.

Acknowledgements

The authors thank Mr. Lucherini Lorenzo for the assistance with SEM-EDX imaging. This work was supported in part by the Swiss National Science Foundation (SNSF Project grant 315230_173243), Swiss Cancer League (No. KFS-4600-08-2018), the European Research Council under the ERC grant agreement MechanoIMM (805337), Kristian Gerhard Jebsen Foundation, and École Polytechnique Fédérale de Lausanne (EPFL). M.G. was in part supported by the China Scholarship Council (CSC) (File No. 201808320453). Y.Z. was supported by the Eurotech Postdoctoral Programme that is cofounded by the European Commission under its framework programme Horizon 2020 (grant agreement 754462). A.K. and X.H. have received funding from the European Union's Horizon 2020 research and innovation programme under the Marie Skłodowska-Curie grant agreement No 754354. S.V.H. was supported by a Ghent University – Special Research Found (BOF) postdoctoral fellowship and FWO travel grant. X.H. was in part supported by the China Scholarship Council (CSC) (File No. 201700260266). Figure 1 was created using elements from BioRender.com.

Conflict of Interest

The authors declare no conflict of interest.

Data Availability Statement

All data supporting the results in this study are available within the Article and its Supplementary Information. The broad range of raw datasets acquired and analyzed (or any subsets of it) are available from the corresponding author on reasonable request.

Keywords

cancer immunotherapy, manganese phosphate nanocluster, STING agonist

Received: March 10, 2021
Revised: May 3, 2021
Published online:

[1] X. Cai, Y. H. Chiu, Z. J. Chen, *Mol. Cell* **2014**, *54*, 289.
[2] Q. Chen, L. Sun, Z. J. Chen, *Nat. Immunol.* **2016**, *17*, 1142.
[3] J. Wu, L. Sun, X. Chen, F. Du, H. Shi, C. Chen, Z. J. Chen, *Science* **2013**, *339*, 826.
[4] D. K. R. Karaolis, T. K. Means, D. Yang, M. Takahashi, T. Yoshimura, E. Muraille, D. Philpott, J. T. Schroeder, M. Hyodo, Y. Hayakawa, B. G. Talbot, E. Brouillette, F. Malouin, *J. Immunol.* **2007**, *178*, 2171.
[5] A. Ablasser, Z. J. Chen, *Science* **2019**, *363*, eaat8657.
[6] T. Ohkuri, A. Kosaka, K. Ishibashi, T. Kumai, Y. Hirata, K. Ohara, T. Nagato, K. Oikawa, N. Aoki, Y. Harabuchi, E. Celis, H. Kobayashi, *Cancer Immunol. Immunother.* **2017**, *66*, 705.
[7] B. S. Pan, S. A. Perera, J. A. Piesvaux, J. P. Presland, G. K. Schroeder, J. N. Cumming, B. Wesley Trotter, M. D. Altman, A. V. Buevich, B. Cash, S. Cemerski, W. Chang, Y. Chen, P. J. Dandliker, G. Feng, A. Haidle, T. Henderson, J. Jewell, I. Kariv, I. Knemeyer, J. Kopinja, B. M. Lacey, J. Laskey, C. A. Lesburg, R. Liang, B. J. Long, M. Lu, Y. Ma, E. C. Minnihan, G. O'Donnell, et al., *Science* **2020**, *369*, eaba6098.
[8] M. Luo, H. Wang, Z. Wang, H. Cai, Z. Lu, Y. Li, M. Du, G. Huang, C. Wang, X. Chen, M. R. Porembka, J. Lea, A. E. Frankel, Y. X. Fu, Z. J. Chen, J. Gao, *Nat. Nanotechnol.* **2017**, *12*, 648.
[9] K. Li, Y. Ye, L. Liu, Q. Sha, X. Wang, T. Jiao, L. Zhang, J. Wang, *Biomater. Sci.* **2021**, *9*, 765.
[10] L. M. Aval, J. E. Pease, R. Sharma, D. J. Pinato, *J. Clin. Med.* **2020**, *9*, 3323.
[11] D. Shae, K. W. Becker, P. Christov, D. S. Yun, A. K. R. Lytton-Jean, S. Sevimli, M. Ascano, M. Kelley, D. B. Johnson, J. M. Balko, J. T. Wilson, *Nat. Nanotechnol.* **2019**, *14*, 269.
[12] S. Chattopadhyay, Y. H. Liu, Z. S. Fang, C. L. Lin, J. C. Lin, B. Y. Yao, C. M. J. Hu, *Nano Lett.* **2020**, *20*, 2246.
[13] S. T. Koshy, A. S. Cheung, L. Gu, A. R. Graveline, D. J. Mooney, *Adv. Biosyst.* **2017**, *1*, 1600013.
[14] Y. Zhang, T. Shen, S. Zhou, W. Wang, S. Lin, G. Zhu, *Adv. Ther.* **2020**, *3*, 2000083.
[15] K. S. Park, C. Xu, X. Sun, C. Louttit, J. J. Moon, *Adv. Ther.* **2020**, *3*, 2000130.
[16] X. Lu, L. Miao, W. Gao, Z. Chen, K. J. Mchugh, Y. Sun, Z. Tochka, S. Tomasic, K. Sadtler, A. Hyacinthe, Y. Huang, T. Graf, Q. Hu, M. Sarmadi, R. Langer, D. G. Anderson, A. Jaklenec, *Sci. Transl. Med.* **2020**, *12*, eaaz6606.
[17] T. Nakamura, H. Miyabe, M. Hyodo, Y. Sato, Y. Hayakawa, H. Harashima, *J. Controlled Release* **2015**, *216*, 149.
[18] D. R. Wilson, R. Sen, J. C. Sunshine, D. M. Pardoll, J. J. Green, Y. J. Kim, *Nanomed. Nanotechnol. Biol. Med.* **2018**, *14*, 237.
[19] J. Zhao, S. Ma, Y. Xu, X. Si, H. Yao, Z. Huang, Y. Zhang, H. Yu, Z. Tang, W. Song, X. Chen, *Biomaterials* **2021**, *268*, 120542.
[20] L. Li, X. Yang, *Oxid. Med. Cell. Longevity* **2018**, *2018*, 7580707.
[21] Z. Zhao, Z. Ma, B. Wang, Y. Guan, X. D. Su, Z. Jiang, *Cell Rep.* **2020**, *32*, 108053.
[22] M. Lv, M. Chen, R. Zhang, W. Zhang, C. Wang, Y. Zhang, X. Wei, Y. Guan, J. Liu, K. Feng, M. Jing, X. Wang, Y. Liu, Q. Mei, W. Han, Z. Jiang, *Cell Res.* **2020**, *30*, 966.
[23] C. Wang, Y. Guan, M. Lv, R. Zhang, Z. Guo, X. Wei, X. Du, J. Yang, T. Li, Y. Wan, X. Su, X. Huang, Z. Jiang, *Immunity* **2018**, *48*, 675.
[24] C. Wang, Z. Sun, C. Zhao, Z. Zhang, H. Wang, Y. Liu, Y. Guo, B. Zhang, L. Gu, Y. Yu, Y. Hu, J. Wu, *J. Controlled Release* **2021**, *331*, 480.
[25] S. L. O'Neal, W. Zheng, *Curr. Environ. Health Rep.* **2015**, *2*, 315.
[26] P. Mi, D. Kokuryo, H. Cabral, H. Wu, Y. Terada, T. Saga, I. Aoki, N. Nishiyama, K. Kataoka, *Nat. Nanotechnol.* **2016**, *11*, 724.
[27] I. Roy, S. Mitra, A. Maitra, S. Mozumdar, *Int. J. Pharm.* **2003**, *250*, 25.
[28] S. Bisso, S. Mura, B. Castagner, P. Couvreur, J. C. Leroux, *Eur. J. Pharm. Biopharm.* **2019**, *142*, 142.

[29] L. Miao, L. Li, Y. Huang, D. Delcassian, J. Chahal, J. Han, Y. Shi, K. Sadtler, W. Gao, J. Lin, J. C. Doloff, R. Langer, D. G. Anderson, *Nat. Biotechnol.* **2019**, *37*, 1174.
[30] Z. S. Liu, Z. Y. Zhang, H. Cai, M. Zhao, J. Mao, J. Dai, T. Xia, X. M. Zhang, T. Li, *Cell Biosci.* **2018**, *8*, 35.
[31] M. Campisi, S. K. Sundararaman, S. E. Shelton, E. H. Knelson, N. R. Mahadevan, R. Yoshida, T. Tani, E. Ivanova, I. Cañadas, T. Osaki, S. W. L. Lee, T. Thai, S. Han, B. P. Piel, S. Gilhooley, C. P. Paweletz, V. Chiono, R. D. Kamm, S. Kitajima, D. A. Barbie, *Front. Immunol.* **2020**, *11*, 2090.
[32] G. Pépin, D. De Nardo, C. L. Rootes, T. R. Ullah, S. S. Al-Asmari, K. R. Balka, H. M. Li, K. M. Quinn, F. Moghaddas, S. Chappaz, B. T. Kile, E. F. Morand, S. L. Masters, C. R. Stewart, B. R. G. Williams, M. P. Gantier, *Mol. Biol. Physiol.* **2020**, *11*, e03187.
[33] O. Demaria, A. De Gassart, S. Coso, N. Gestermann, J. Di Domizio, L. Flatz, O. Gaide, O. Michielin, P. Hwu, T. V. Petrova, F. Martinon, R. L. Modlin, D. E. Speiser, M. Gilliet, *Proc. Natl. Acad. Sci. USA* **2015**, *112*, 15408.
[34] A. Cachot, M. Bilous, Y. Liu, X. Li, A. Rockinger, M. Saillard, T. Wyss, P. Guillaume, J. Schmidt, R. Genolet, M. P. Protti, W. Reith, L. De Leval, K. Ioannidou, G. Coukos, A. Harari, D. Speiser, A. Mathis, D. Gfeller, H. Altug, P. Romero, C. Jandus, *Sci. Adv.* **2021**, *7*, eabe3348.
[35] R. P. Robert, *Mayo Clin. Proc.* **2004**, *79*, 91.
[36] P. M. Herst, C. Grasso, M. V. Berridge, *Cancer Metastasis Rev.* **2018**, *37*, 643.
[37] L. Hou, C. Tian, Y. Yan, L. Zhang, H. Zhang, Z. Zhang, *ACS Nano* **2020**, *14*, 3927.
[38] J. Chandra, S. M. Teoh, P. Kuo, L. Tolley, A. A. Bashaw, Z. K. Tuong, Y. Liu, Z. Chen, J. W. Wells, C. Yu, I. H. Frazer, M. Yu, *J. Immunol.* **2021**, *206*, 987.
[39] R. Kedmi, N. Ben-Arie, D. Peer, *Biomaterials* **2010**, *31*, 6867.
[40] L. Corrales, L. H. Glickman, S. M. McWhirter, D. B. Kanne, K. E. Sivick, G. E. Katibah, S. R. Woo, E. Lemmens, T. Banda, J. J. Leong, K. Metchette, T. W. Dubensky, Jr., T. F. Gajewski, *Cell Rep.* **2015**, *4*, 1018.